FFI-rapport 2014/01927

Detection performance for Incoherent Range Walk Compensation

Erlend Finden, Jonas Myhre Christiansen,
Øystein Lie-Svendsen and Karl Erik Olsen

FFI Forsvarets forskningsinstitutt

Detection performance for Incoherent Range Walk Compensation

Erlend Finden, Jonas Myhre Christiansen, Øystein Lie-Svendsen and Karl Erik Olsen

Norwegian Defence Research Establishment (FFI)

24 November 2014

FFI-rapport 2014/01927

1297

P: ISBN 978-82-464-2462-0
E: ISBN 978-82-464-2463-7

Keywords

Radar

Avstands-spredning

Approved by

Karl Erik Olsen	Project manager
Johnny Bardal	Director

English summary

FFI supports the Royal Norwegian Air Force in their acquisition of new air surveillance sensors. Improved detection performance on low observable targets may be obtained by increasing the radar dwell time on target. For each doubling of integration time the theoretical maximum improvement is 3 dB for coherent integration and between 1.5 and 3 dB for incoherent integration. However, increased integration time yields a risk of range and Doppler walk, which decreases the detection performance. An algorithm to incoherently compensate for range walk, is applied on real data from a passive bistatic radar utilizing digital video broadcasting television transmitters. With the algorithm the detection threshold for a given false alarm rate is lowered as the integration time is extended. Thus, targets below the detection threshold for coherent integration, can with the compensation algorithm, be above the corresponding detection threshold. For the single target studied, the method was found to give between 1.5 and 3 dB for each doubling of the integration time. The method is only successful for targets with little Doppler walk. Moreover, the integration time in the method is limited by the amount of Doppler walk and in our test the method gave no detection improvement after 4.2 s integration time, due to Doppler walk. The method has here been studied on a single target only, thus no conclusions should be drawn on other configurations before a statistical study has been performed.

Sammendrag

FFI støtter Luftforsvaret i anskaffelsen av nye sensorer for militær luftromsovervåking i prosjektprogram Luftmilitær Overvåking. Økt deteksjonsytelse på mål med lavt radartversnitt kan oppnås ved hjelp av lengre integrasjonstid. En forventet teoretisk maksimal økning i deteksjonsytelse er 3 dB for hver dobling av integrasjonstiden ved koherent integrasjon, og mellom 1.5 og 3 dB ved inkoherent integrasjon. Lengre integrasjonstid øker imidlertid risikoen for range og Doppler-spredning, som senker deteksjonsytelsen. En metode som kompenserer range-spredning inkoherent, er anvendt på reelle data fra en passiv bistatisk radar som utnytter TV-sendere i det digitale bakkenettet. Med algoritmen kan deteksjonsterskelen for en gitt falsk-alarmrate senkes mens integrasjonstiden økes. Mål som befinner seg under deteksjonsterskelen ved koherent integrasjon, kan med algoritmen komme over denne terskelen. Metoden ga mellom 1.5 og 3 dB for hver dobling av integrasjonstiden, i samsvar med teorien. Metoden er kun anvendelig på mål med lite Doppler-spredning. Videre er integrasjonstiden med metoden begrenset av når Doppler-spredning eventuelt inntreffer. For målet som ble studert her, ga derfor metoden ingen økning i deteksjonsytelse etter 4.2 s integrasjonstid, grunnet Doppler-spredning. Resultatene vist her er kun fra et enkelt mål, og det kan ikke konkluderes med hvorvidt metoden er egnet for å øke deteksjonsytelsen for mål med lite Doppler-spredning generelt.

Contents

1 Introduction

Air surveillance sensors may face new threats such as low observable targets. Improved detection performance on such low observable targets can be achieved by spending more time on target, which allows prolonged integration time. Prolonged integration time is also essential if Non Cooperative Target Recognition (NCTR) techniques are desired. Certain radar types may offer the so called backscan opportunity in order to achieve prolonged integration time. This feature allows to observe a suspect search volume a second time by electronically steering the radar beam back into the search volume of interest while the antenna rotates (1). However, prolonged integration time also introduces a risk of energy dispersal in both the range and Doppler dimensions, referred to as range and Doppler walk, respectively. Range walk occurs when a target migrates over more than one range cell during the integration time (2). The risk for range walk to occur increases with higher bandwidth, which corresponds to a finer range resolution. The risk also increases with increasing integration time and with increasing radial target velocity with respect to the radar. Targets with a radial velocity component with respect to the radar will experience increased range walk as the integration time is increased. When present, range walk decreases the ratio between the target energy and the noise (3).

For Doppler walk, it is likewise. Doppler walk occurs when a target migrates over more than one Doppler cell during the coherent integration time. The risk for Doppler walk to occur is dependent on the acceleration of the target with respect to the radar, and the Doppler resolution. In practice, targets will often experience both range and Doppler walk. Methods that compensate for range walk only, will be successful only for targets with little Doppler walk, since Doppler walk causes the range walk compensation to break down.

The point in time at which Doppler walk becomes significant limits how long a target can be integrated with range walk compensation only, without Doppler walk compensation. The issue of Doppler walk is not considered in this report. Detection theory is here applied to evaluate the benefit obtained by an existing range walk compensation method. Methods to compensate for range walk can be either coherent or incoherent. The incoherent method is expected to give less gain than the coherent method (4). However, the incoherent method is also expected to be less computational demanding since Fast Fourier Transform (FFT) methods can be applied in the signal processing, therefore only the incoherent method is studied.

A Passive Bistatic Radar (PBR) utilize transmitters of opportunity (e.g. broadcast transmitters), which transmit continuously. This yields a duty cycle of 100%. Moreover, the desired surveillance volume can be covered 100% of the time with the PBR receiver antennas. Hence, PBR systems are well suited to study prolonged integration times with 100% time on target (5). Recently, PBR has operated with integration times of approximately 1 s in order to achieve the desired integration gain (3). This is relatively long compared with classic monostatic radars (5). Moreover, PBR utilizing Digital Video Broadcasting - Terrestrial (DVB-T) signals can also operate with a range resolution down to 40 m or less. These PBRs are likely to observe targets which undergo range walk.

Monostatic radars that apply prolonged integration time will have to perform signal processing similar to that of a PBR system. The results presented here should thus also be relevant to monostatic radar systems that apply long integration times.

2 Method

Data from a PBR was used in this work. The sensor is capable of receiving and sampling several Radio-Frequency (RF) signals simultaneously. The system operates in the Ultra High Frequency (UHF) band, and utilize DVB-T transmitters as illuminators of opportunity. One reference and one surveillance antenna with corresponding channels are applied in the signal processing. Both antennas are regular yagi TV-antennas (Fig. 2.1). The reference antenna was pointed towards the

Figure 2.1 A picture of the radar receiver antennas with the surveillance antennas on top and the reference antenna below.

Tryvasshøgda DVB-T transmitter, and the two surveillance antennas were pointed towards the Oslo Gardermoen (OSL) Airport. Both the reference and the surveillance antennas were located at the Norwegian Defense Research Establishment (FFI). The DVB-T channel 52 was utilized. This channel has 8 MHz bandwidth and a center frequency of 722 MHz. The receiver unit down-converts the radio frequency signal to 68 MHz where it is sampled at 64 MHz and stored on a hard drive

disk. Furthermore, the data are digitally filtered with an 8 MHz rectangular filter and digitally down converted such that the resulting complex signal is located between -4 MHz and 4 MHz. Moreover, the data are decimated such that the sampling frequency of the stored data is 8 MHz. The processing algorithm follows the efficient range-Doppler processing presented by (5).

The signal in the reference and surveillance channels is expressed as

$$r(i), \quad i = 1, \cdots, S \tag{2.1}$$

and

$$s(i), \quad i = 1, \cdots, S \tag{2.2}$$

respectively, where S is the length of the reference and surveillance data channels. Furthermore, the Range-Doppler (rD)-map is given by the 2D-Cross Correlation Function (2D-CCF)

$$|\tilde{\chi}(l, m)| = |\sum_{k=0}^{S-1} r(k)s^*(k + l)e^{-\imath 2\pi km/S}| \tag{2.3}$$

Here l is the time index, m is the bistatic Doppler index, s^* denotes the complex conjugate of s and $\imath = \sqrt{-1}$. The time index l is related to the time delay τ expressed as follows

$$\tau = l/f_s \tag{2.4}$$

where f_s is the sampling frequency of the stored data and the coherent integration time t_c is expressed as

$$t_c = S/f_s \tag{2.5}$$

Moreover, the bistatic Doppler index m is related to the Doppler frequency f_D, i.e.

$$f_D = f_s m/S \tag{2.6}$$

The delay τ is referred to as the bistatic time difference of arrival (6). (7) defines τ as

$$\tau = \frac{R_B}{c} \tag{2.7}$$

where R_B is the relative bistatic range, which in the following will be referred to as bistatic range. In a PBR, the bistatic range can be related to the geometry of the receiver, transmitter and target (Fig. 2.2), by the following expression

$$R_B = Rt + Rr - L \tag{2.8}$$

Here the target is at the distance Rt from the transmitter and at the distance Rr from the receiver. The distance between the transmitter and the receiver is denoted L.

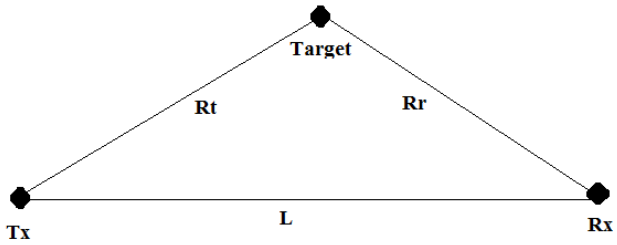

Figure 2.2 The geometry of a PBR illustrating the signal path from the transmitter (Tx) to the target and to the receiver denoted Rt and L, respectively. The reflected signal path Rr from the target to the receiver (Rx) is also illustrated.

In this work (2.3) is simplified to obtain computational efficiency by a method referred to as Batches Algorithm (7). This method yields an integration loss that is Doppler dependent (8). In (8) the Batches Algorithm is reviewed and it is shown that the 2D-CCF can be rearranged in the form

$$|\tilde{\chi}(l,m)| = |\sum_{i=0}^{A-1}(\sum_{n=0}^{N-1} r(n+iN)s^*(n+iN+l)e^{-\imath 2\pi m\frac{n}{S}})e^{-\imath 2\pi m\frac{i}{A}}| \tag{2.9}$$

where $S = AN$, $A > 0$ and $N > 0$ are integers. The Batches Algorithm neglects the inner exponential term of (2.9), i.e.

$$|\tilde{\chi}(l,m)| \approx |\chi(l,m)| \equiv |\sum_{i=0}^{A-1} e^{-\imath 2\pi m\frac{i}{A}} \sum_{n=0}^{N-1} r(n+iN)s^*(n+iN+l)| \tag{2.10}$$

This method of calculating the rD-map is referred to as an Frequency Modulated Continuous Wave (FMCW)-Like Approach in (6), and Decimation Technique in (8). An expression for the maximum achievable gain for a target at $l = l'$ and $m = m'$ for signals with a unitary amplitude is presented in (8). However, we stress that for a DVB-T signal, the modulus of the complex weights at the different sub-carriers for instance in a 64-Quadrature Amplitude Modulation (QAM) signal, are not constant for all the points in the constellation map, and thus would not have a unitary amplitude (9). Nevertheless this assumption serves as an indicator of the behavior of the Doppler dependent

loss arising from the simplification taken in the Batches Algorithm. In (8) they first assume that the only contribution in the surveillance channel is a delayed and Doppler shifted replica of the reference channel signal, which is scaled in amplitude with a factor $\alpha \in [0, 1)$, i.e.

$$s(n + iN + l') = \alpha r(n + iN) e^{\imath 2\pi (n+iN) \frac{f_D}{f_s}} \tag{2.11}$$

Hence

$$|\chi(l', m')| = |\alpha \sum_{i=0}^{A-1} \sum_{n=0}^{N-1} r(n + iN) r^*(n + iN) e^{-\imath 2\pi (n+iN) f_D/f_s} e^{-\imath 2\pi m' \frac{i}{A}}| = |\alpha \sum_{i=0}^{A-1} \sum_{n=0}^{N-1} ||r(n + iN)||^2 e^{-\imath 2\pi n f_D/f_s} e^{-\imath 2\pi i (N f_D/f_s + \frac{m'}{A})}| \tag{2.12}$$

Substituting (2.6) in (2.12) yields

$$|\chi(l', m')| = |\alpha \sum_{i=0}^{A-1} \sum_{n=0}^{N-1} ||r(n + iN)||^2 e^{\imath 2\pi n m'/S}| \tag{2.13}$$

We here assume $||r(n + iN)||^2 = 1$, hence

$$|\chi(l', m')| = |\alpha A \sum_{n=0}^{N-1} e^{\imath 2\pi n m'/S}| = \begin{cases} \alpha S & m' = 0 \\ \alpha A |\frac{1 - e^{\imath 2\pi m' N/S}}{1 - e^{\imath 2\pi m'/S}}| = \alpha A |\frac{\sin(\frac{\pi}{A} m')}{\sin(\frac{\pi}{S} m')}| & m' \neq 0 \end{cases} \tag{2.14}$$

Here the sum was written out as a geometric series. Considering the expression (2.14), for $m' \in \{-A/2, .., 0, .., A/2 - 1\}$ the minima of χ as a function of Doppler is achieved when $m' = -A/2$ or $m' = A/2$.

When $m' = -A/2$, it becomes

$$|\chi(l', -A/2)| = \alpha A |\frac{-1}{\sin(-\frac{\pi}{2} \frac{1}{N})} \approx \alpha \frac{2}{\pi} S \tag{2.15}$$

Here we assume that $N >> 1$. Hence the approximation in (2.10) reduces $|\chi|$ by a factor of maximum $2/\pi$.

We express (2.14) for $m' \neq 0$ as a function of Doppler frequency by the relation (2.6) and divide with αS in order to plot the reduction as a function of f_D, i.e.

$$20 \log_{10} |\chi(l', f_D)| = 20 \log_{10} \frac{1}{N} |\frac{\sin(\frac{\pi f_D N}{f_s})}{\sin(\frac{\pi f_D}{f_s})}| \tag{2.16}$$

For typical processing parameters applied in this work, the loss given by (2.16) increases with Doppler frequency f_D (Fig. 2.3).

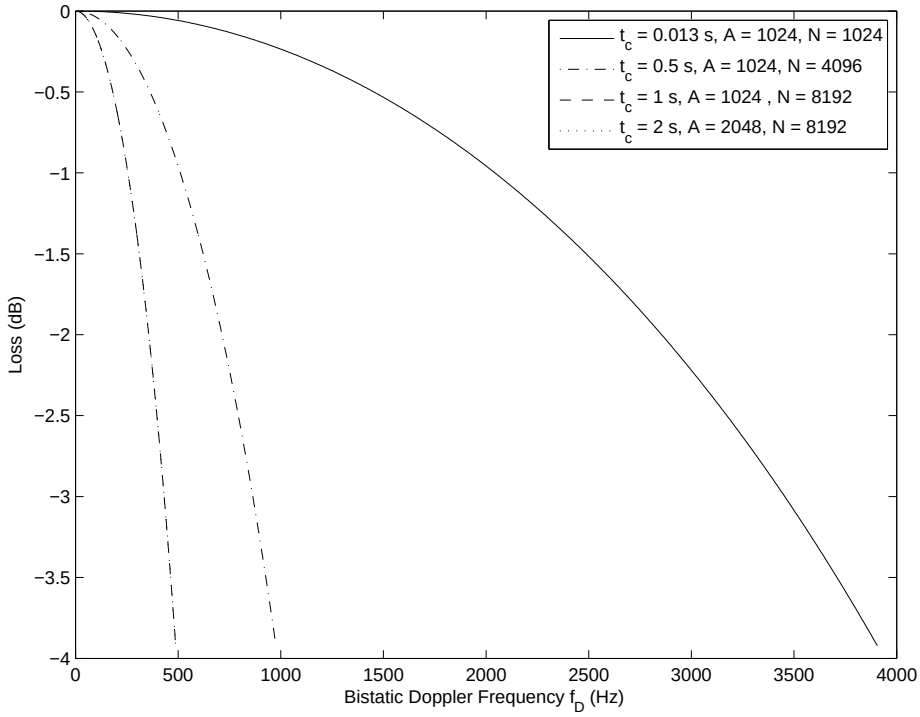

Figure 2.3 The loss introduced by the Batches Algorithm (2.16) for a unitary amplitude signal for a target located at $l = l'$ and $m = m'$. The plots are symmetric about the y-axis.

In contrast, the corresponding 2D-CCF (2.3) with a target consisting of a delayed, scaled and Doppler-shifted replica of the direct signal can be expressed as

$$|\chi(l', m')| = |\alpha \sum_{n=0}^{S-1} s(n + l')e^{\imath 2\pi m' n/S} s^*(n + l')e^{-\imath 2\pi m' n/S}| = \alpha S \tag{2.17}$$

when assuming unitary amplitude of the signal.

Let us define the Signal-to-Noise Ratio (SNR) of element l, m as

$$SNR(l, m) = 10 \log_{10}(\frac{|\chi(l, m)|^2}{< |U_0| >}) \tag{2.18}$$

where

$$U_0 = \chi^2(l,m), \quad l = \{P, \cdots, K\} \textit{ and } m = \{-L/2, \cdots, L/2-1\} \tag{2.19}$$

The K, P and L are parameters to be chosen later.

The processing parameters for coherent integration applied in this work is given in table 2.1.

Table 2.1 The processing parameters for coherent integration.

t_c	A	N
Coh. int. time	No. of Doppler elements	No. of range elements
0.013 s	1024	1024
0.25 s	1024	2048
0.52 s	1024	4096
1.0 s	1024	8192
2.1 s	2048	8192
4.2 s	4096	8192
8.4 s	8192	8192

2.1 Range Walk Compensation

In order to utilize long integration times, range and Doppler walk must be compensated. In (3) the authors introduced an expression to incoherently compensate range walk where velocity information in the rD-map is utilized. Assuming that the targets have little Doppler walk (little bistatic acceleration), the velocity information and the coherent integration interval are applied to estimate the range migration, which in turn is compensated in each Doppler column. The argument in the expression for the range walk compensated rD-map by (3), can be squared in order to have a closed form expression for the corresponding noise probability distribution, i.e.

$$\hat{\chi}(l,m) = \sum_{k=0}^{M-1} |\chi(l - \lfloor \frac{f_s m k}{f_c} \rfloor, m)_k|^2 \tag{2.20}$$

Here χ_k represents a rD-map that is integrated coherently over a time interval k with length t_c. Moreover, f_c is the carrier frequency, and f_s is the sampling frequency. The floor operator is denoted $\lfloor x \rfloor$ and rounds down x to the nearest integer. Let us denote the total incoherent integration interval with this method $T_I = Mt_c$. t_c is here chosen as long as possible without causing range walk for a target of interest. In the following we refer to (2.20) as Incoherent Range Walk Compensation (IRWC).

Let us define the SNR of element l, m in the method as

$$SNR(l,m) = 10\log_{10}(\frac{\hat{\chi}(l,m)}{<|U_1|>}) \tag{2.21}$$

Here

$$U_1 = \hat{\chi}(l,m), \quad l = \{P, \cdots, K\} \textit{ and } m = \{-L/2, \cdots, L/2-1\} \tag{2.22}$$

Note that with coherent integration the Doppler resolution becomes finer proportional to the integration time, but with the IRWC-method the Doppler resolution is given by the coherent integration time t_c only. The integration time is thus prolonged without achieving finer Doppler resolution. Hence, with the IRWC-method, Doppler walk does not distribute target energy in Doppler to the same extent as with coherent integration over the same integration time T_I.

In this report the benefit of the IRWC-method is measured with detection thresholds. As the incoherent integration time is extended, the detection threshold is observed to be lowered due to less relative fluctuation of noise signals. Moreover, the benefit of the IRWC-method is compared with coherent integration by calculating the ratio between the peak target values and the corresponding detection thresholds for the two methods. The expected benefit of the IRWC-method is a higher ratio due to a lower threshold. In order to calculate such thresholds, statistical information about the noise is required. We define the representative noise samples for coherent integration and for the IRWC-method as U_0 given in (2.19) and U_1 given in (2.22), respectively.

We choose K, L and P in (2.19) and (2.22) based on the following considerations: The sidelobes of (2.10) increase with both range and Doppler. This is apparent when a synthetic DVB-T signal is inserted in both r and s in (2.10) to obtain the Ambiguity Function (AF) (Fig. 2.4-2.5). For $f_c = 722$ MHz, the noise floor varies less in range from 20 to 105 km (approximately 1 dB) than in Doppler out to $\pm$ 1 kHz (approximately 5 dB). Moreover, for the targets we consider, the bistatic detection range does not exceed 105 km. To avoid strong clutter and targets at short range, we therefore choose $K = 540$ and $P = 2800$ in U_0 and U_1, corresponding to a range from 20 to 105 km. In Doppler we choose to apply a span of 100 Doppler columns in the vicinity of the target Doppler frequency as a representative sample of noise, which must be selected such that deterministic peaks in the DVB-T AF are avoided. Hence, the representative noise samples of the rD-map depend on the target Doppler. For a target at -340 Hz and a Doppler resolution $f_D = 1.92$ Hz, we choose $L = 100$ Doppler columns that correspond to the Doppler frequencies from -456 to -264 Hz.

As will be shown (implicit) later, the noise in both the real and the imaginary part of the complex χ in (2.19) are normal distributed. Taking the modulus $|\chi|$ and squared modulus $|\chi|^2$ of these complex elements yields a Rayleigh and an exponential distribution of the elements, respectively, (4). The exponential Probability Density Function (pdf) is described in terms of the β-parameter, and reads

$$\rho(x) = \beta e^{-\beta x} \tag{2.23}$$

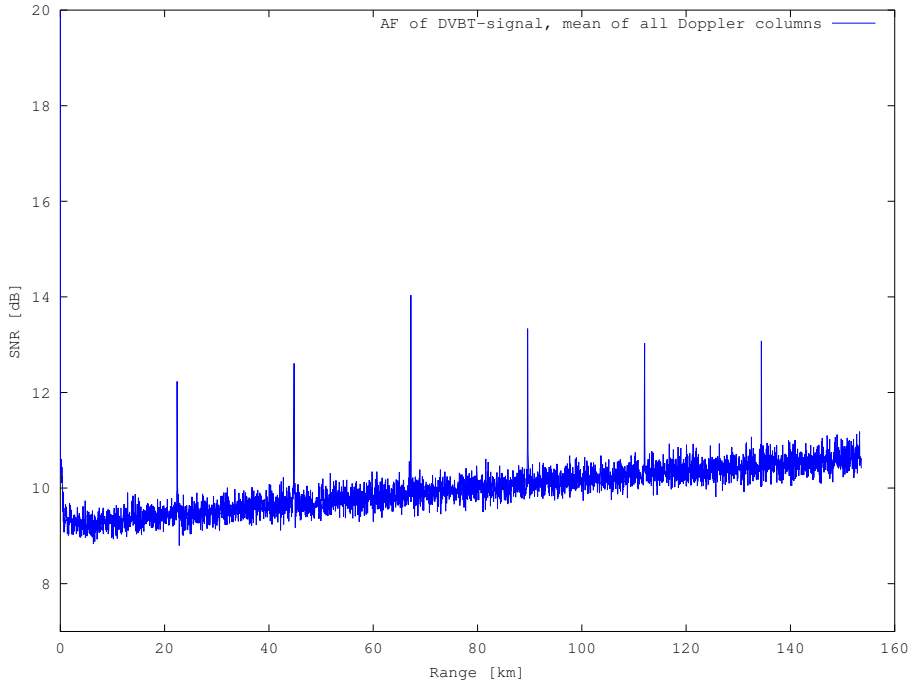

Figure 2.4 The AF of a synthetic DVB-T signal in (2.18) averaged over all Doppler columns as a function of range. $t_c = 0.52$ *s,* $A = 1024$ *and* $N = 4096$.

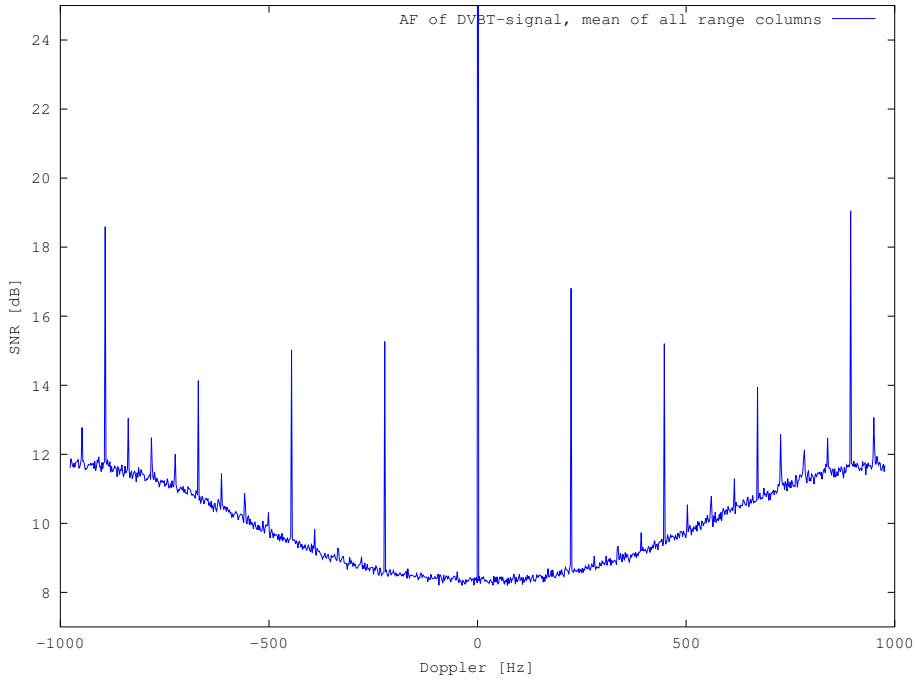

Figure 2.5 The AF of a synthetic DVB-T signal in (2.18) averaged over all range columns as a function of Doppler. $t_c = 0.52$ *s,* $A = 1024$ *and* $N = 4096$.

where $x \in [0, \infty)$ and β is related to the mean by

$$\beta^{-1} =< x > \tag{2.24}$$

The sum of M independent exponentially distributed random variables with the same scale parameter β, as in the IRWC-method (2.20), are recognized as a gamma distribution also called the Special Erlangian distribution (10), which is defined as

$$\rho(x) = \frac{\beta^M x^{M-1} e^{-\beta x}}{\Gamma(M)} \tag{2.25}$$

Increasing the total integration time in (2.20) corresponds to higher values of M in the distribution (2.25). To show that the relative appearance of x with high values in the distribution decrease with increasing M, we make a change of variable, i.e.

$$\rho(\frac{x}{< x >}) =< x > \frac{\beta^M (\frac{x}{<x>})^{M-1} e^{-\beta(\frac{x}{<x>})}}{\Gamma(M)} \tag{2.26}$$

Relative to the average $< x >$, the distribution (2.25) has fewer higher values of x as M increases for $\beta = 1$ (Fig. 2.6).

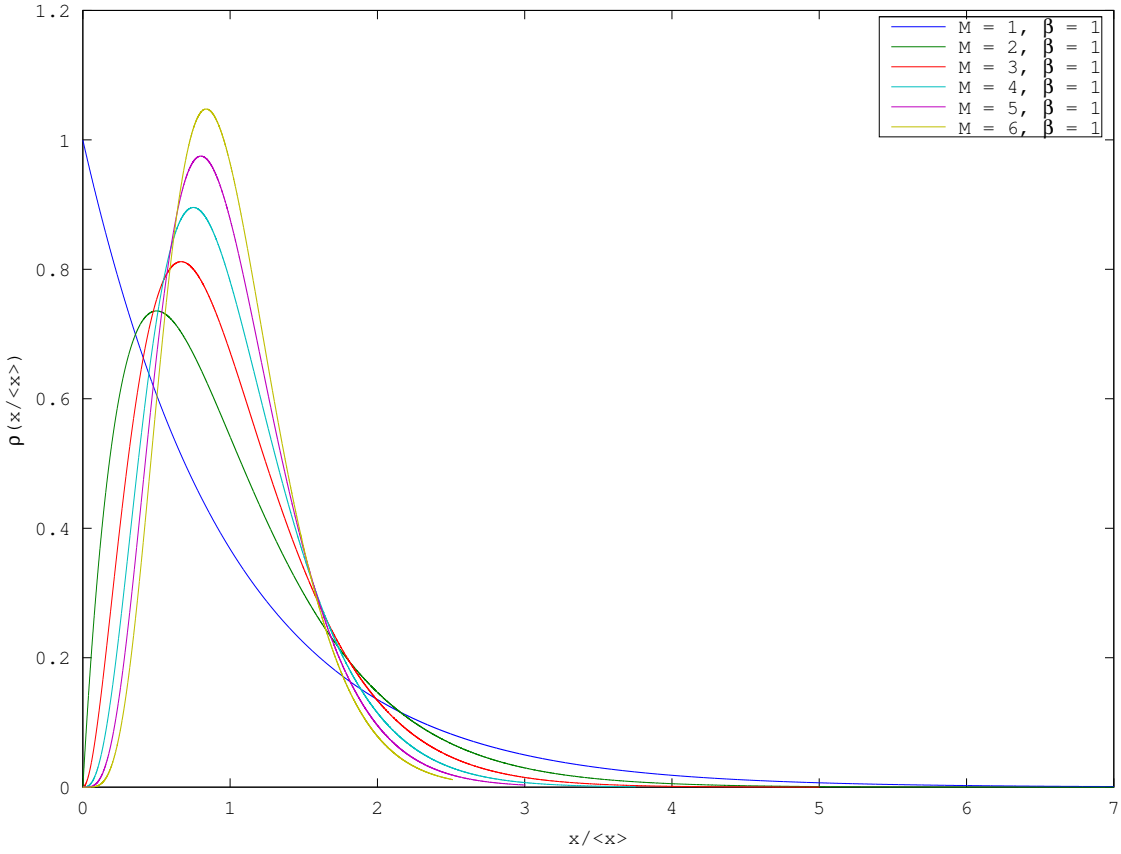

Figure 2.6 The Special Erlangian distribution with a change of variable $\rho(\frac{x}{<x>})$ in (2.26).

For a given probability of false alarm P_{FA}, the detection threshold x_T is obtained from

$$\int_{x_T}^{\infty} \rho(x)dx = P_{FA} \tag{2.27}$$

Considering first the exponential distribution, from (2.27) and (2.23) we get

$$x_{TC} = \frac{\ln(P_{FA})}{-\beta} \tag{2.28}$$

Here x_{TC} denotes the coherent integration threshold.

By integration by parts, (2.27) for the IRWC-method can be expressed as

$$P_{FA}e^{\beta x_{TI}} = \sum_{j=1}^{M} \frac{(\beta x_{TI})^{M-j}}{(M-j)!} \tag{2.29}$$

Here β is calculated by (2.24), and x_{TI} denotes incoherent integration detection threshold. The transcendental equation (2.29) can be solved numerically with respect to x_{TI}.

Let us define the target-to-threshold ratio for coherent integration as follows:

$$\Delta_C = 10\log_{10}(\frac{|\chi(l',m')|^2}{x_{TC}}) \tag{2.30}$$

Here the target has a peak magnitude at range bin l' and Doppler bin m'. Likewise for the IRWC-method:

$$\Delta_I = 10\log_{10}(\frac{\hat{\chi}(l',m')}{x_{TI}}) \tag{2.31}$$

3 Results

Both coherent integration and the IRWC-method are here applied to a single target detected by the PBR sensor located at FFI. With coherent integration (2.18) and $t_c = 4.2$ s the target energy is smeared out in range due to range walk, while with $t_c = 0.52$ s the target experience little range walk (Fig. 3.1). The target is distributed over approximately 5 Hz in Doppler for both integration times. Thus, this particular target does not experience increased Doppler walk as the integration time is increased. However, the finer Doppler resolution with a longer coherent integration time causes the energy to be distributed over more Doppler bins.

When coherent integration by (2.18) of 6 intervals with length $t_c = 0.52$ s are performed, the target shows only a slight decrease in Doppler frequency in the first 6 seconds (Fig. 3.2).

Plots of SNR (2.18) as a function of range with the Doppler frequency fixed at -340 Hz shows that target SNR is smeared out in range as the coherent integration time t_c increases due to range walk (Fig. 3.3).

The peak target SNR calculated by (2.18) first increases with the coherent integration time, but then decreases after 0.52 s due to range walk (Fig. 3.4). With no range and Doppler walk, the SNR should increase linearly with t_c (4).

The peak target SNR is approximately equal for coherent integration by (2.18) with $t_c = 0.52$ s and for the IRWC-method (2.21) with $T_I = 2.1$ s (Fig. 3.5). This is consistent with the general fact that incoherent integration does not lead to an increase in the SNR. However, the relative noise fluctuation decreases (as also indicated in Fig. 3.5). Still, the peak SNR both for coherent integration with $t_c = 0.52$ s and the IRWC-method with $T_I = 2.1$ s are higher than for coherent integration with $t_c = 2.1$ s, where range walk is present.

In (3) the coherent integration time t_c was varied while the total integration time T_I was held fixed for the IRWC-method. The authors plotted SNR as a function of M. It was found that there was a peak in SNR for the M corresponding to the maximum integration time that did not cause range

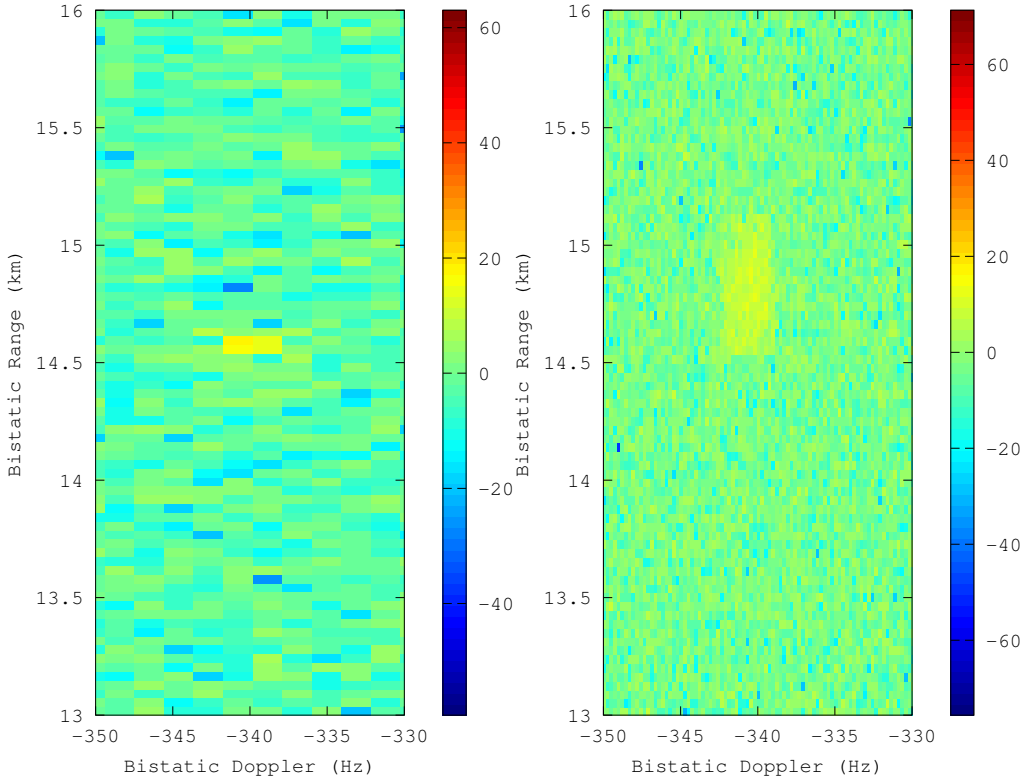

Figure 3.1 *The target shown in rD-map by (2.18).*
Left image: Coherent integration time $t_c = 0.52$ s. Doppler resolution $\Delta f_D = 1.92$ Hz.
Right image: $t_c = 4.2$ s and $\Delta f_D = 0.24$ Hz.

walk. Both a real and a simulated target showed this behavior. We therefore examined range walk compensation only with this optimal coherent integration time, which is approximately 0.52 s in our work, (Fig. 3.4).

Histograms and pdf-models for the representative noise samples U_0 in (2.19) and U_1 in (2.22) around the target are calculated for coherent integration (Fig. 3.6) and for the IRWC-method (Fig. 3.7). The noise distributions follow the analytic expressions for the two pdfs rather closely, also for the highest signal levels. This justifies the use of the analytic expressions for the respective distributions to calculate the thresholds.

With the pdf obtained from the exponential distribution (Fig. 3.6) and $P_{FA} = 10^{-6}$, (2.28) yields the threshold $x_{TC} = 13.82$. Likewise, with the parameters applied in Fig. 3.7, (2.29) was solved numerically with respect to x_{TI}, yielding $x_{TI} = 21.35$.

The benefit of the IRWC-method, which is a lower threshold for the same P_{FA}, is apparent when the thresholds and the corresponding SNR-plots are compared (Fig. 3.8). Weaker targets that would be

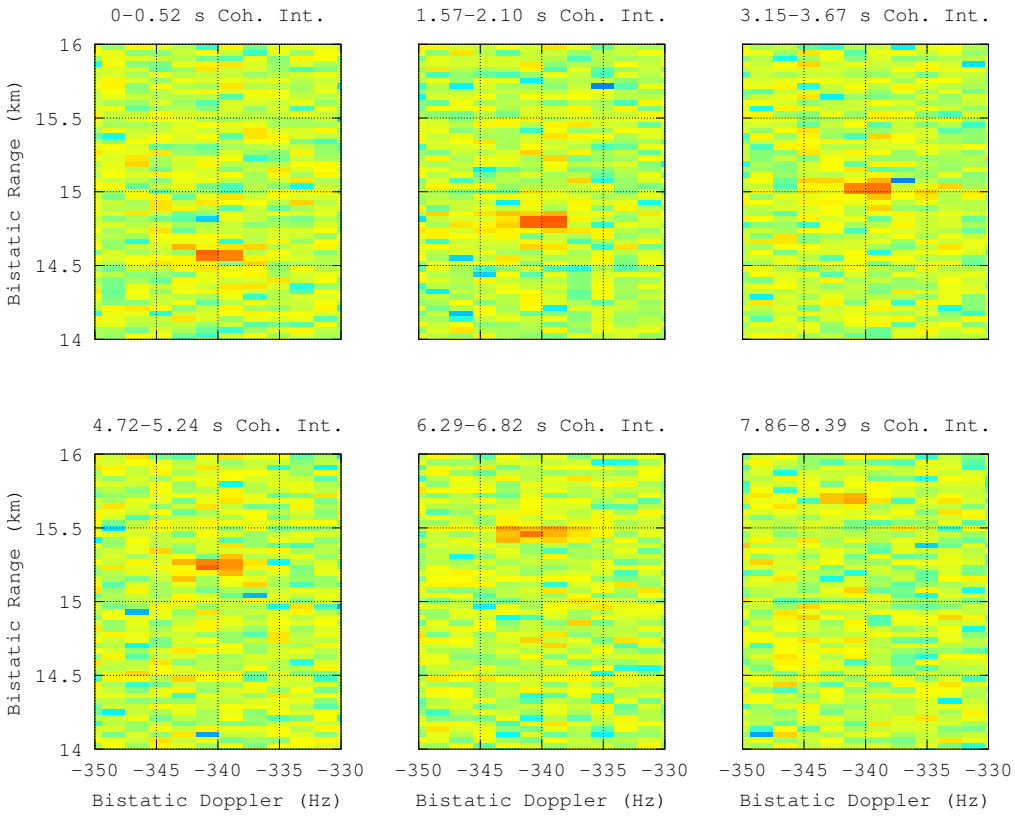

Figure 3.2 The target shown in rD-maps by (2.18) with $t_c = 0.52$ s for each subplot. The orange color corresponds to rD-elements with high amplitudes.

classified as noise with coherent integration, can be detected with the IRWC-method.

Solutions of (2.28)-(2.31) with $\beta^{-1} =< |U_0| >$ are summarized in Table 3.1.

Table 3.1 The ratio between peak target magnitude and detection thresholds.

Method	P_{FA}	Total int. time	Length of IRWC: M	Target-threshold-ratio: Δ
Coherent integration	10^{-5}	0.52 s	-	7.3 dB
Coherent integration	10^{-6}	0.52 s	-	6.5 dB
IRWC-method	10^{-6}	1.0 s	2	8.5 dB
IRWC-method	10^{-5}	2.1 s	4	11.1 dB
IRWC-method	10^{-6}	2.1 s	4	10.6 dB
IRWC-method	10^{-6}	4.2 s	8	11.6 dB
IRWC-method	10^{-6}	8.4 s	16	11.6 dB

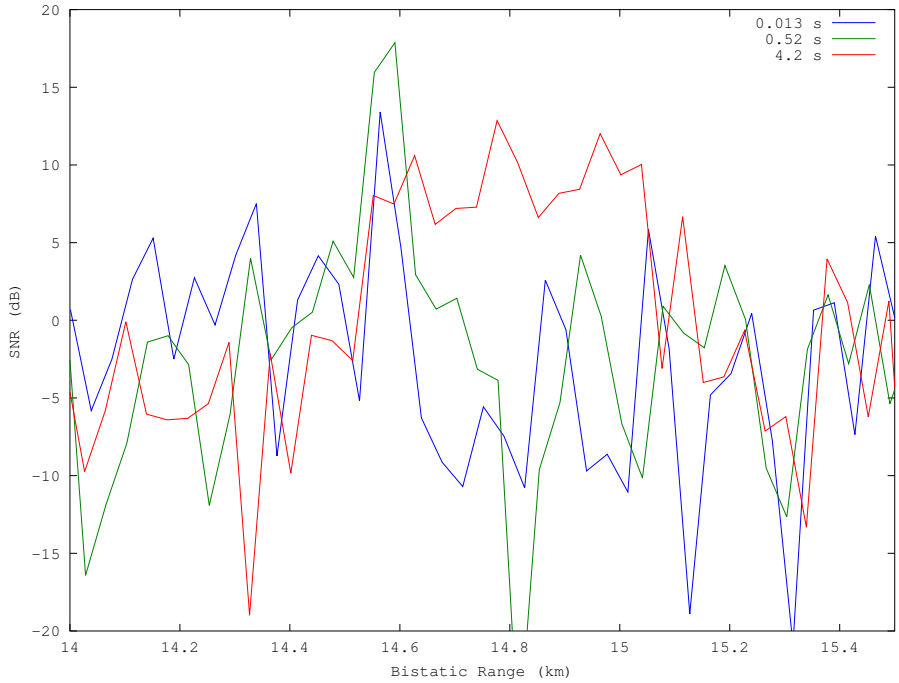

Figure 3.3 The SNR as a function of range at a fixed Doppler frequency of -340 Hz. The coherent integration times t_c are 0.013 s, 0.52 s and 4.2 s (see Table 2.1).

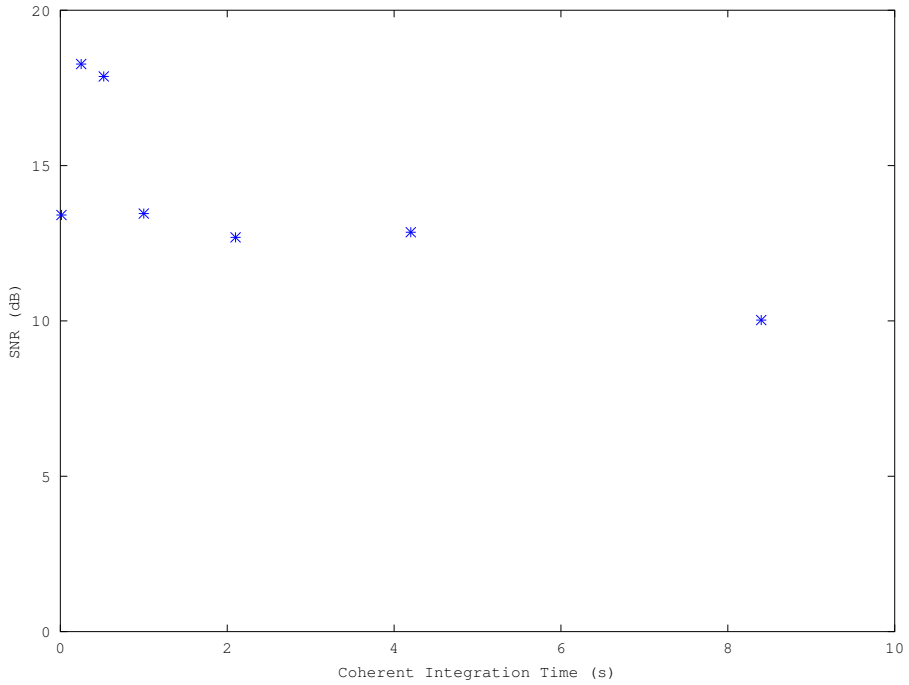

Figure 3.4 The peak value of the target SNR as a function of the coherent integration time, t_c.

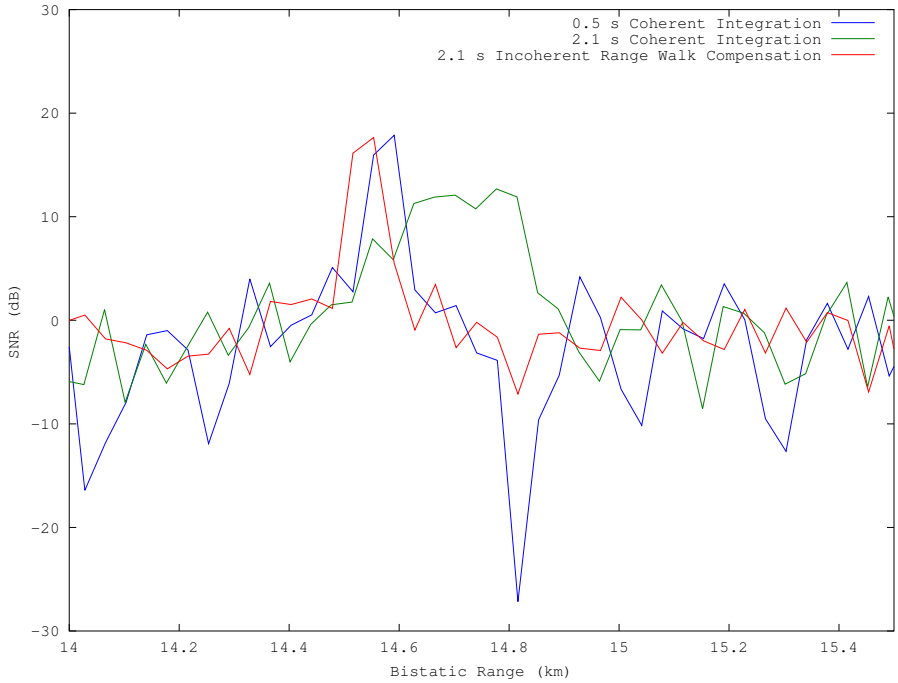

Figure 3.5 The SNR as a function of bistatic range while the bistatic Doppler is kept fixed at -340 Hz. 2.1 s IRWC, 2.1 s coherent integration and 0.52 s coherent integration.

Regarding the difference between $P_{FA} = 10^{-5}$ and $P_{FA} = 10^{-6}$ for 0.52 s coherent integration and for 2.1 s IRWC, the enhancement in target-to-threshold ratio is approximately 4 dB for both (Table 3.1).

The threshold x_{TI} for $P_{FA} = 10^{-6}$ decreases as M increases. However, due to Doppler walk, the peak target SNR also decrease from 4.2 s to 8.4 s (Fig. 3.9).

For $P_{FA} = 10^{-6}$ the enhancement in target-to-threshold ratio with the IRWC-method compared with 0.52 s coherent integration is observed to be between $\sqrt{M}$ and M (Fig. 3.10), as is expected for incoherent integration (4). In contrast, the gain achieved in coherent integration is expected to be proportional to the integration time (4). Since the target changes Doppler after 7 s (see Fig. 3.2), the method gives no enhancement between $M = 8$ (4.2 s) and $M = 16$ (8.4 s), (Fig. 3.10). Hence, further enhancement after 4.2 s of integration is not possible without also doing Doppler walk compensation.

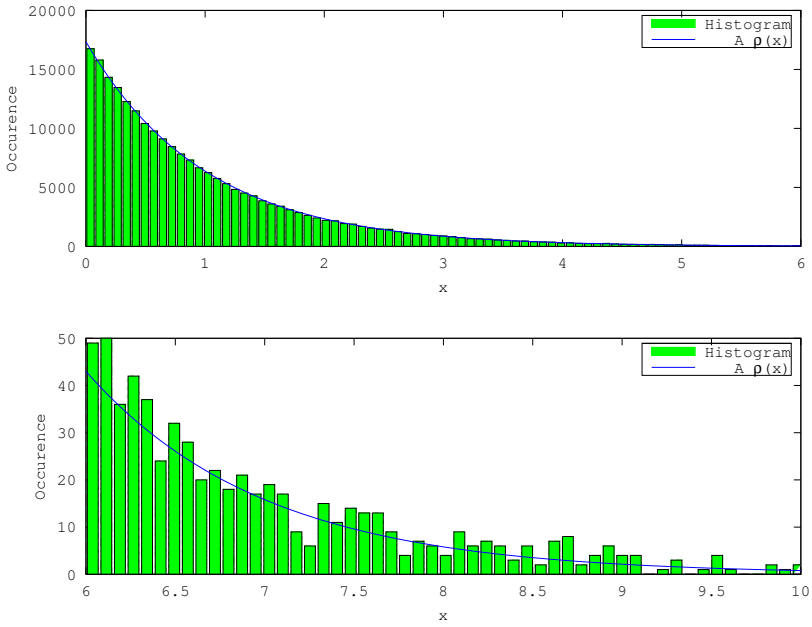

Figure 3.6 *Upper Fig.: A histogram of the representative noise sample around the target at* $f_D = -340$ *Hz from coherent integration (2.19), presented as* $x = \frac{|U_0|}{<|U_0|>}$ *and a plot of* $\rho(x)$ *from (2.23) multiplied by the area* A *under the histogram.* $\beta^{-1} =< x >$ *and* $t_c = 0.52$ *s. The number of samples is* 228361.
Lower Fig.: The tail of the histogram in the upper Fig. is showing the highest values.

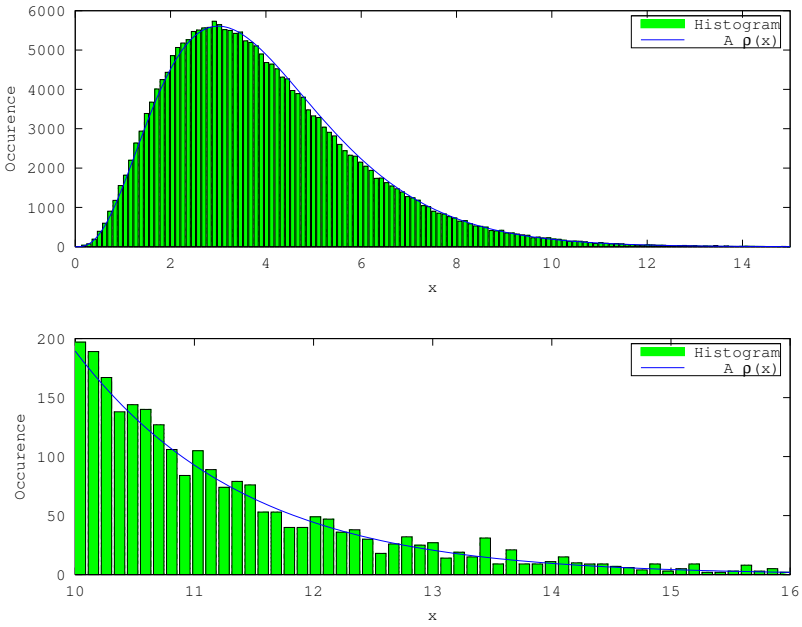

Figure 3.7 *Upper Fig.: A Histogram of the representative noise sample around the target at* $f_D = -340$ *Hz from IRWC-method (2.22), presented as* $x = \frac{|U_1|}{<|U_0|>}$ *and a plot of* $\rho(x)$ *from (2.25) multiplied by the area* A *under the histogram.* $M = 4$ *and* β *are defined as in Fig. 3.6.* $t_c = 0.52$ *s and* $T_I = 2.1$ *s. The same total number of samples as in Fig. 3.6 is used.*
Lower Fig.: The tail of the histogram in the upper Fig. is showing the highest values.

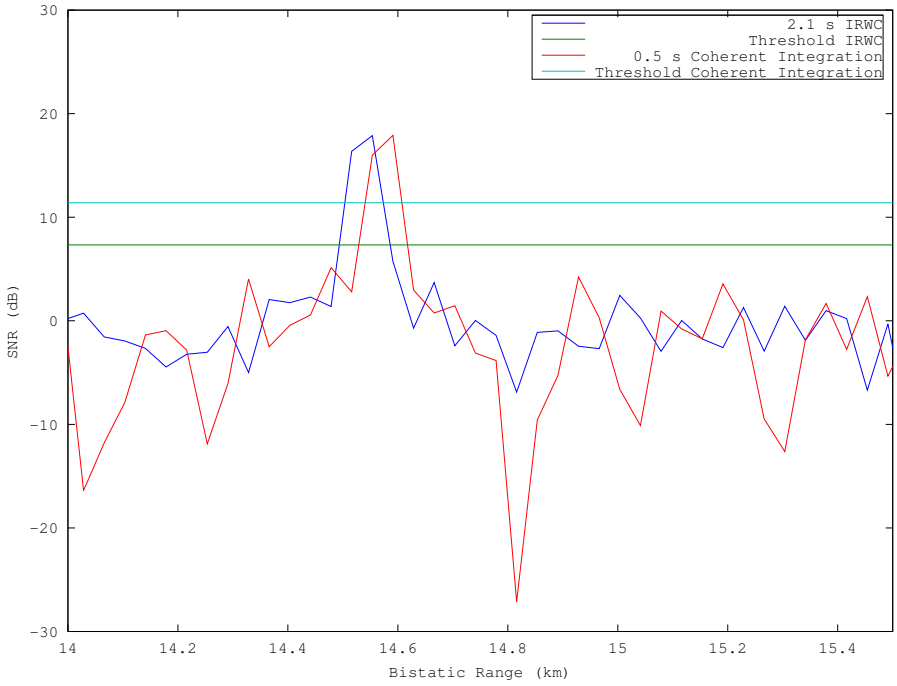

Figure 3.8 The SNR as a function of bistatic range while the bistatic Doppler is kept fixed at -340 Hz. 2.1 s IRWC and 0.5 s coherent integration. The thresholds for $P_{FA} = 10^{-6}$ are also shown.

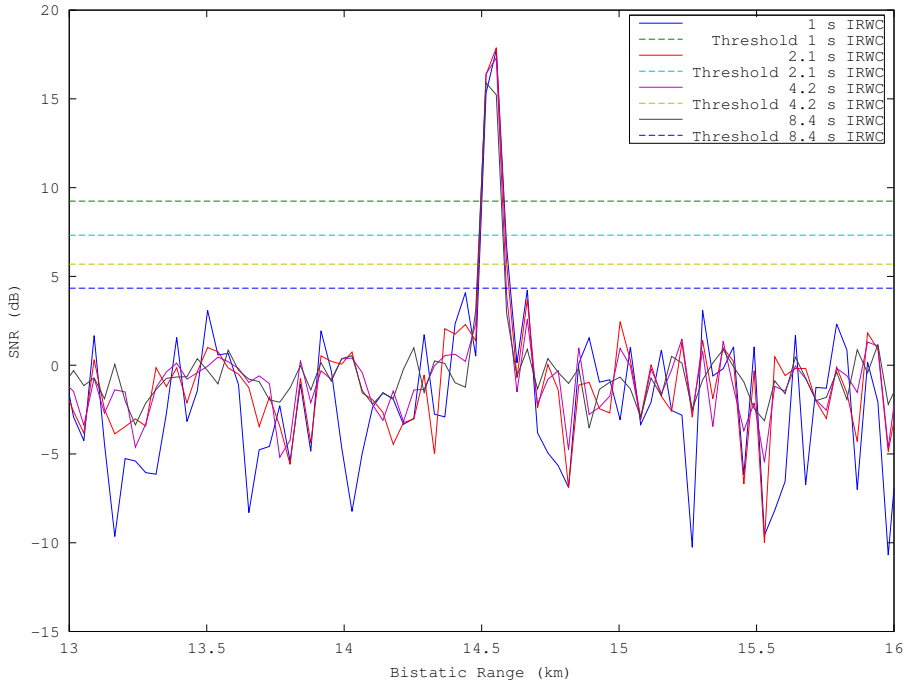

Figure 3.9 The SNR for the IRWC-method as a function of bistatic range while the bistatic Doppler is kept fixed at -340 Hz. $T_I = 1.0$ s, 2.1 s, 4.2 s and 8.4 s with corresponding thresholds for $P_{FA} = 10^{-6}$.

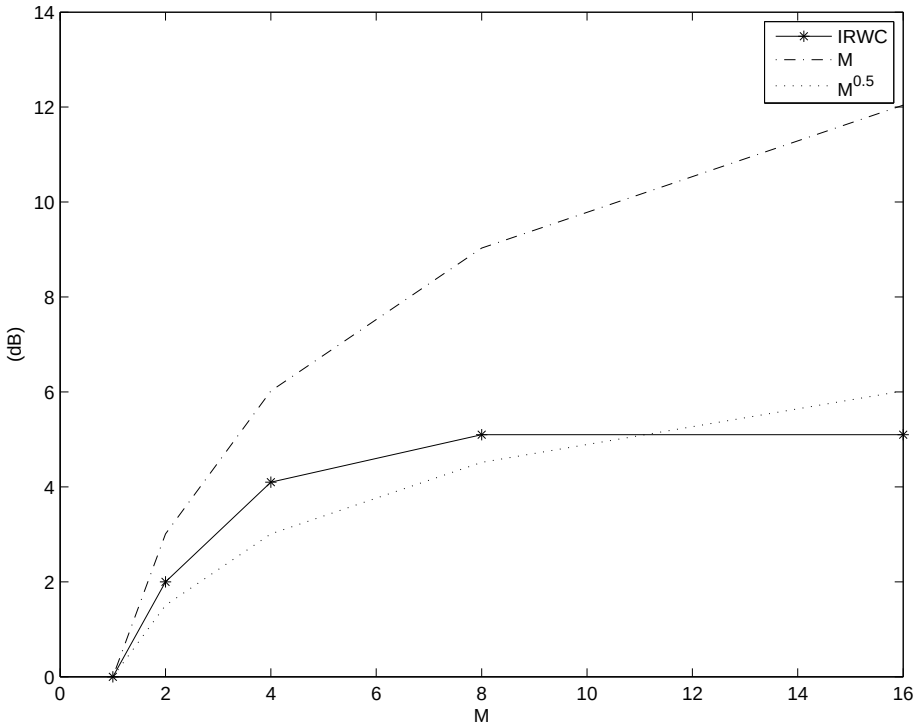

Figure 3.10 A plot of the enhancement in target-to-threshold ratio with the IRWC-method compared with 0.52 s coherent integration ($M = 1$), M and $\sqrt{M}$. The data are from Table 3.1.

4 Discussion

Targets close to the zero-Doppler line may not experience range walk at the coherent integration intervals that cause range walk for targets at higher Doppler frequencies. Signals from these targets can be integrated coherently for a longer time before range walk causes a decrease in SNR, and the maximum SNR achievable with coherent integration will be higher for these targets. Hence optimum t_c depends on target Doppler. In (11) it is therefore suggested to apply different integration intervals in different regions of the rD-map. Thus coherent integration may be applied to regions near zero-Doppler, and the IRWC-method may be applied in nonzero Doppler regions.

Although the IRWC-method will work for targets with constant bistatic velocity, targets with bistatic acceleration will in addition to range walk exhibit Doppler walk. Hence targets near the zero-Doppler may be coherently integrated without any range walk, but still have a spread in energy due to Doppler walk. If the target of interest has zero acceleration with respect to the radar, thus no Doppler walk, the integration time T_I may be extended as long as desired with the IRWC-method. However, in practice targets will finally change speed or direction relative to the radar, and have a nonzero acceleration. This is observed after 7 s (Fig. 3.2), hence the benefit does not increase between $M = 8$ (4.2 s) and $M = 8$ (8.4 s), (Fig. 3.10).

5 Conclusion and Outlook

With a combination of high bandwidth, high target velocity and long integration time, range walk will occur and lead to an energy dispersal. The detection performance of an incoherent method to compensate range walk was here studied. By adding, incoherently, the rD-matrices of M consecutive coherent integration intervals, the ratio between the peak magnitude of the target and the threshold for a given false alarm rate was increased. As a function of M, the enhancement in this ratio increased less than M and above $\sqrt{M}$, with highest rate at low numbers of M. This is as expected from theory. Although for this particular target there was a detection improvement by the IRWC-method, more targets must be studied before a conclusion about the method can be drawn.

Since the IRWC-method only provides range walk compensation, only targets with little Doppler walk will take advantage of it. The limit for how long one may integrate with the method is set by the time for which Doppler walk becomes present. For the target studied here, the method gave no increase in detection performance from 4.2 s to 8.4 s integration time, due to Doppler walk. Hence, in addition to range walk compensation, also Doppler walk compensation is desirable, but more difficult because the rD-map does not provide information about target acceleration, which requires tracking.

In future work it will be natural to also study range walk compensation with coherent integration, as in (12). Although range walk compensation with coherent integration is expected to be more complex and require more computational power, it will yield a higher gain than incoherent integration.

References

[1] H. Meikle., *Modern Radar Systems,* . Artech House, 2008.

[2] A. Partizian, *Principles of Modern Radar: Advanced Techniques*, ch. Electronic Protection. Edison, NJ: SciTech Publishing., 2013.

[3] J. M. Christiansen and K. E. Olsen, "Range and Doppler walk in DVB-T based passive bistatic radar," in *Radar Conference, 2010 IEEE*, pp. 620–626, IEEE, 2010.

[4] M. A. Richards., *Principles of Modern Radar - Basic Principles*. Raleigh, NC.: SciTech Publishing., 2010.

[5] K. E. Olsen, *Investigation of bandwidth utilisation methods to optimise performance in passive bistatic radar*. PhD thesis, UCL (University College London), 2011.

[6] P. E. Howland, H. D. Griffiths and C. J. Baker., *Bistatic Radar - Emerging Technology*, ch. Passive Bistatic Radar Systems. The Atrium, Southern Gate, Chichester, West Sussex PO19 8SQ, England.: John Wiley & Sons Ltd., 2008.

[7] P. Lombardo and F. Colone, *Principles of Modern Radar: Advanced Techniques*, ch. Advanced Processing Methods for Passive Bistatic Radar Systems. Edison, NJ: SciTech Publishing., 2013.

[8] D. Langellotti, F. Colone, C. Bongioanni, and P. Lombardo, "Comparative study of ambiguity function evaluation algorithms for passive radar," in *International Radar Symposium. IRC. Hamburg, Germany, September 9-11, 2009.*, 2009.

[9] W. Fischer, *Digital Video and Audio Broadcasting Technology, A Practical Engineering Guide*. Berlin Heidelberg: Springer-Verlag, 2 ed., 2008.

[10] E. Lloyd, *Handbook of Applicable Mathematics Volume 2 - Probability , BASIC PRINCIPLES*. John Wiley & Sons Ltd., 1980.

[11] J. M. Christiansen, "DVB-T based Passive Bistatic Radar," Master's thesis, Norwegian University of Science and Technology, 2009.

[12] M. Malanowski, K. Kulpa, and K. Olsen, "Extending the integration time in DVB-T-based passive radar," in *Radar Conference (EuRAD), 2011 European*, pp. 190–193, IEEE, 2011.

[13] "IEEE Standard Definitions, IEEE Std 686-1997 (Revision of IEEE Std 686-1990), Institute of Electrical and Electronics Engineers (IEEE) Std., 1997. [Online]." `http://www.ieee.org`.

[14] H. Kuschel and D. O'Hagan, "Passive radar from history to future," in *IEEE Radar Symposium (IRS)*, IEEE, 2010.

List of Acronyms

AF Ambiguity Function
DVB-T Digital Video Broadcasting - Terrestrial
FFI Norwegian Defense Research Establishment
FFT Fast Fourier Transform
FMCW Frequency Modulated Continuous Wave
IRWC Incoherent Range Walk Compensation
NCTR Non Cooperative Target Recognition
OSL Oslo Gardermoen
PBR Passive Bistatic Radar
pdf Probability Density Function
QAM Quadrature Amplitude Modulation
RF Radio-Frequency
rD Range-Doppler
SNR Signal-to-Noise Ratio
UHF Ultra High Frequency
2D-CCF 2D-Cross Correlation Function

Appendix A Passive Bistatic Radar

The IEEE define a bistatic radar as: “A radar using antennas for transmission and reception at sufficiently different locations that the angles or ranges from those locations to the target are significantly different” (13). Furthermore is passive bistatic radar (PBR) defined in (6) as a “variant of bistatic radar that exploit ”illuminators of opportunity” as their sources of radar transmission“. Examples of illuminators of opportunity are television and radio broadcasting transmitters (6). In fact, aircraft detection by passive radar was demonstrated as early as 1935 by Sir Robert Watson-Watt utilizing the BBC Empire shortwave transmitter at Daventry (14).

One PBR signal processing approach is to cross-correlate a radio-frequency signal directly received from a transmitter with the same signal that has been reflected from a target, (14). One transmitter antenna and two dedicated receiver antennas can be used. A reference antenna with a beam directly on the transmitter antenna will receive the transmitted signal directly. This antenna together with the surveillance antenna constitute the receiving antennas. The surveillance antenna has the main lobe pointing away from the transmitter and towards air targets. The signal from the transmitter antenna is here propagated in different directions. Thus, the signal from the transmitter is reflected both from buildings, ground and targets towards the two surveillance antennas. The transmitted signal that is reflected from the air targets and then into the main lobe of the surveillance antenna, is delayed compared with the signal received in the reference antenna that comes directly from the transmitter. This delay together with the distance between the receiver and transmitter antennas can be used to calculate the so called bistatic range. With additional azimuth and elevation information, the position of the target can be determined.